THE JOURNAL OF PHYSICAL CHEMISTRY B
A JOURNAL OF THE AMERICAN CHEMICAL SOCIETY

pubs.acs.org/JPCB

Article

# Association–Dissociation Dynamics of Ionic Electrolytes in Low Dielectric Medium

*Published as part of The Journal of Physical Chemistry virtual special issue "Kankan Bhattacharyya Festschrift".*

Deborin Ghosh, Sushil S. Sakpal, Srijan Chatterjee, Samadhan H. Deshmukh, Hyejin Kwon, Yung Sam Kim,* and Sayan Bagchi*

Cite This: *J. Phys. Chem. B* 2022, 126, 239–248

Read Online

ACCESS | Metrics & More | Article Recommendations | Supporting Information

**ABSTRACT:** Ionic electrolytes are known to form various complexes which exist in dynamic equilibrium in a low dielectric medium. However, structural characterization of these complexes has always posed a great challenge to the scientific community. An additional challenge is the estimation of the dynamic association–dissociation time scales (lifetime of the complexes), which are key to the fundamental understanding of ion transport. In this work, we have used a combination of infrared absorption spectroscopy, two-dimensional infrared spectroscopy, molecular dynamics simulations, and density functional theory calculations to characterize the various ion complexes formed by the thiocyanate-based ionic electrolytes as a function of different cations in a low dielectric medium. Our results demonstrate that thiocyanate is an excellent vibrational reporter of the heterogeneous ion complexes undergoing association–dissociation dynamics. We find that the ionic electrolytes exist as contact ion pairs, dimers, and clusters in a low dielectric medium. The relative ratios of the various ion complexes are sensitive to the cations. In addition to the interactions between the thiocyanate anion and the countercation, the solute–solvent interactions drive the dynamic equilibrium. We have estimated the association–dissociation dynamics time scales from two-dimensional infrared spectroscopy. The exchange time scale involving the cluster is faster than that between a dimer and an ion pair. Moreover, we find that the dynamic equilibrium between the cluster and another ion complex is correlated to the solvent fluctuations.

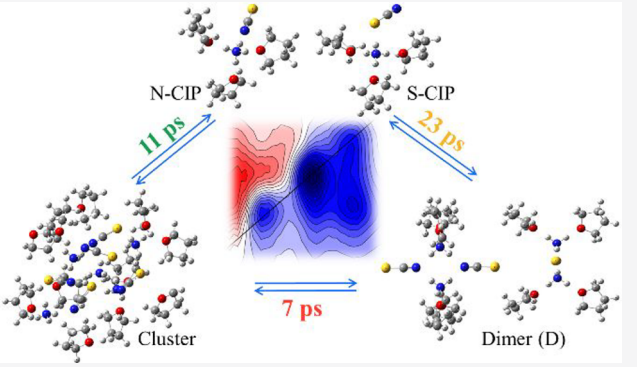


## 1. INTRODUCTION

In the last few decades, demand for renewable and alternate energy sources and storage media has grown exponentially.[1] Although the state of the art lithium-ion battery is widely used at present, high demand, inefficient performance in large-scale energy storage systems, and scarcity of raw material require exploring a more diverse range of alternative metal cation electrolyte systems.[2−5] Fortunately, a re-emergence of various metal-cation ($Na^+$, $K^+$, $Zn^{2+}$, and various multivalent cations) batteries, judicious designing of nonaqueous to polymer electrolyte systems, and ion-conducting membranes are paving the way for the future.[6−8] However, a molecular-level understanding of the electrolyte systems is paramount toward improving the ion conductivity and charge transfer kinetics, providing a wider electrochemical window.[9−12]

The fundamental understanding is vital because many of the proposed electrolytes tend to form ion pairs and aggregates.[13] The formation of different ion complexes that negatively contribute to ion transport has also been shown to be extremely sensitive toward the dielectric constant of the solvent.[14,15] Despite having many favorable properties like durability and high electrochemical stability, ion complex formation is one of the main reasons polymer electrolytes are still lagging behind conventional liquid-based electrolyte systems in terms of ion transport.[3,16] The low dielectric constant of the polymer electrolyte favors the ion complex formation and, in turn, limits the ion diffusion constant.[17−20] Interestingly, a recent study by Gudla and co-workers has proposed that the formation of complexes and the lifetimes of such complexes (the association–dissociation rate) determine the ion transport rate.[15] They have shown that depending on the dielectric constant of the medium, the rate of the ion complex formation can be modulated, and only the longer-

Received: September 30, 2021
Revised: December 7, 2021
Published: December 28, 2021

lived complexes hinder the ion transport.[15] Thus, deciphering the identities of different ion complexes and estimating their association−dissociation rates in a low dielectric medium is crucial to our fundamental understanding.

To date, different spectroscopic and electrochemical techniques like infrared (IR) spectroscopy, Raman spectroscopy, and dielectric relaxation spectroscopy have been extensively used to understand solvation structure and ion complex formation in various protic and aprotic solvents of varying polarity.[21−25] Together with ab initio electronic structure theory calculations, such experimental techniques can identify different ion complexes, such as a contact ion pair (CIP), dimer, and ion cluster in solution.[13] However, these time-averaged experimental techniques cannot measure the ion complexation lifetime in solution and the effect of the solvent dynamics on the ion complex stability. In this regard, two-dimensional infrared (2D IR) spectroscopy, with femtosecond time resolution, is well-suited to monitor the time evolution of energetically distinct ion complexes in solution and allows quantitative investigation of the role of solvent fluctuations toward the dynamic equilibrium within ion complexes.[26−30]

The concentrated aqueous electrolyte solution has been previously studied using 2D IR spectroscopy to extract the population exchange rate of ion-pair dynamics.[29−31] 2D IR studies of the interconversion between ion pair and cluster systems in different aqueous electrolytes indicate that the ultrafast exchange rate is highly dependent on the nature of the cation.[29,31−33] A strongly interacting cation like lithium induces the slowest interconversion rate.[29,30,34] Intriguingly, ion-pair dynamics in nonaqueous solvent using thiocyanate as a vibrational probe unravel markedly different ion cluster population ratios with distinct interconversion rates than the aqueous counterpart.[30,34−36] Molecular dynamics (MD) simulation has also been extensively used to identify the molecular picture and the interconversion rate in different ion complex systems.[37−40] For example, classical and quantum MD simulations have been used to predict the temperature-dependent effect of local composition and dynamics of hydrated calcium ion in solution.[40] Free energy calculations have been used to identify different ion solvent complex structures of their relative stability in a low dielectric solvent like THF.[39] 2D IR and extensive MD simulations on a thiocyanate vibrational probe with different countercations have been used to understand molecular picture of ion association and dissociation in aqueous medium.[41] However, a molecular-level understanding of ion complex formation and the association−dissociation dynamics in a low dielectric medium is still lacking. A combined approach of MD simulations and ultrafast IR spectroscopy could provide us with the much-needed microscopic picture.

In this paper, we have used the nitrile stretch of thiocyanate ($SCN^-$) ion as a vibrational probe to identify the interactions and dynamics of various ion complexes in a low dielectric solvent tetrahydrofuran (THF). We have varied the countercations from the strongly coordinating sodium ($Na^+$) and potassium ($K^+$) to a weakly coordinating cation like ammonium ($NH_4^+$) with diffused charge density. Interestingly, the $SCN^-$ nitrile stretch is shown to be an excellent probe to identify cation-specific population ratios of different associated ion complexes. The cation-specific ion complexes are further analyzed using MD simulations. Representative snapshots of different ion complexes from MD simulations are further extracted to calculate the nitrile stretch frequency using ab initio quantum chemical calculations. The excellent agreement between computed and the experimental frequencies of different ion complexes provides a complete molecular picture of the electrolyte solution.

Moreover, 2D IR spectroscopy has been performed to obtain the ion complex formation−dissociation rates by monitoring the time evolution of the cross peaks as a function of waiting time. The ultrafast rate of interconversion between different ion complexes was found to be highly specific to the nature of the complexes. This rate of interconversion, coupled with the knowledge of the solvent fluctuation time scale and a molecular picture from MD simulation, provides us a detailed molecular-level description of the electrolyte system.

## 2. MATERIALS AND METHODS

**2.1. Materials.** Ammonium thiocyanate ($NH_4SCN$), sodium thiocyanate (NaSCN), potassium thiocyanate (KSCN), methyl thiocyanate (MeSCN), and tetrahydrofuran (THF) were purchased from Sigma-Aldrich. All these chemicals were used without further purification.

**2.2. Linear IR Spectroscopy.** IR absorption spectra were acquired on a Bruker Vertex 70 spectrometer with a 2 $cm^{-1}$ resolution at room temperature. For all samples, 100 $\mu$L of the sample solution was loaded into a demountable cell (PIKE Technologies) consisting of two $CaF_2$ windows with 3 mm in thickness (Shenzhen Laser) separated by a Mylar spacer of 100 $\mu$m thickness. The spectrometer was purged with dry air. The baseline corrected spectra of the solute were obtained by subtracting the pure solvent spectrum from the absorption spectrum of the nitrile stretch of the thiocyanate salt in respective solutions. In every case, broad asymmetric IR signals were observed. Peak positions were obtained from the second derivative of the IR spectra. The IR spectra were then fitted with the known peak positions using Voigt line shape profiles and the underlying peaks were reconstructed from the fitting parameters.

**2.3. Laser System and Optical Setup.** A detailed description of the setup used for this work was described previously.[42] In brief, a Ti:sapphire regenerative amplifier (50 fs pulse-width at 800 nm, 1 kHz repetition rate) was used to pump an optical parametric amplifier (OPA). The signal (1363.96 nm) and idler (1900.63 nm) were focused at the difference frequency generation ($AgGaS_2$) crystal to produce mid-IR pulses (~7 $\mu$J at 2070 $cm^{-1}$, 170 $cm^{-1}$ bandwidth). This ultrashort mid-IR pulse has been directed to the 2D IR spectrometer (PhaseTech) where the pulse was split into a strong pump (80%) and a weak probe (20%) beam. The pump pulse was passed through a germanium acousto-optic modulator (AOM)-based pulse shaper which generates a collinear pair of compressed pump pulses with variable delays ($\tau$) that are scanned to generate the pump axis (excitation frequencies) of the 2D IR spectra. The pump and probe pulses were spatially overlapped and focused at the sample position using parabolic mirrors. At a fixed temporal delay between the pump and the probe pulses (waiting time, $T_w$), $\tau$ was scanned to generate the 2D IR signal. The signal was dispersed with a monochromator (Princeton Instruments) and detected on a liquid nitrogen-cooled 64 element IR array detector (InfraRed Associates). All 2D IR spectra have been collected at 22 °C temperature. The sample cells for 2D IR experiments have been prepared in the same manner as that for the IR absorption experiments. For NaSCN and $NH_4SCN$, the 2D IR experiments were performed with ~70 mM concentration in


https://doi.org/10.1021/acs.jpcb.1c08613
J. Phys. Chem. B 2022, 126, 239−248

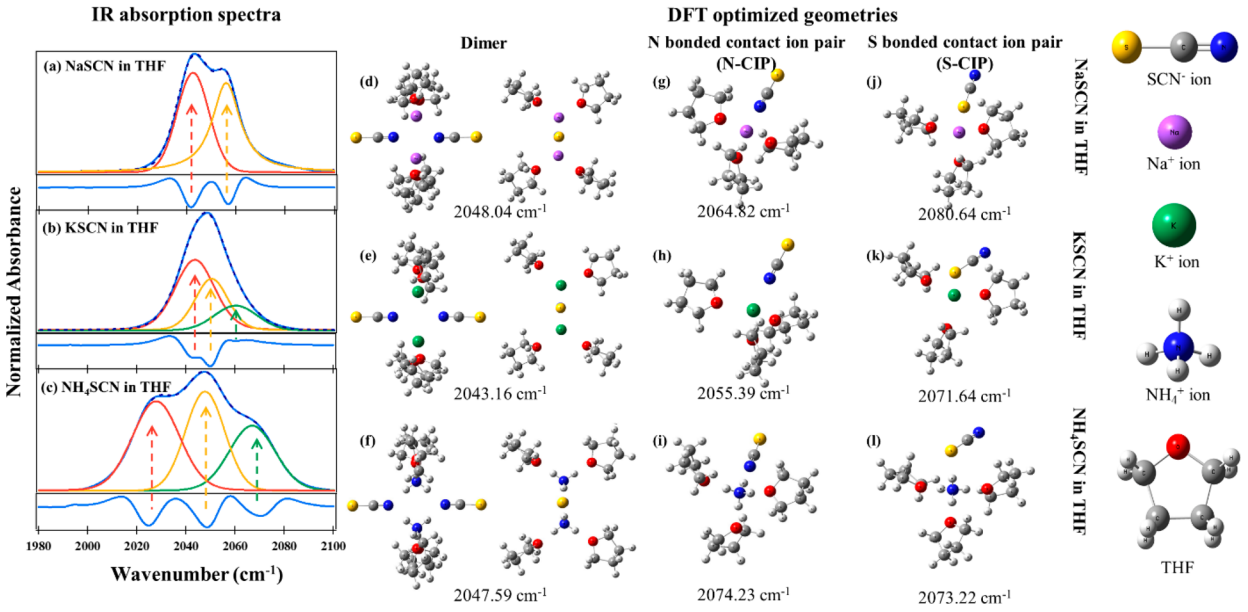


**Figure 1.** IR absorption spectra of (a) NaSCN, (b) KSCN, and (c) $NH_4SCN$ in THF show overlapping transitions. The spectra were fitted to multiple peaks using Voigt line shape profiles. The peak positions were obtained from the second derivatives (shown at the bottom of each IR spectrum) of the IR spectra. The underlying peak represents the ion-pair dimer (red) and the contact ion pair (yellow). In addition, the blue-shifted peak (green) was observed in KSCN and $NH_4SCN$. The DFT optimized structures and nitrile stretch frequencies are for the (d–f) dimer, (g–i) N-bonded contact ion pair, and (j–l) S-bonded contact ion pair. The optimized dimer structures are shown both from the top and the side.

THF. A saturated solution of the sparingly soluble KSCN was used for the 2D IR experiments.

**2.4. 2D IR Spectrum.** The 2D IR spectrum is a correlation spectrum between the excitation and the detection frequencies. For a single population, a typical 2D IR spectrum consists of a peak pair; a diagonal peak (blue) arising from v = 0 → v = 1 transitions and another peak (red) arising from v = 1 → v = 2 transitions. The red peak is shifted along the detection frequency axis by the vibrational anharmonicity. In the case of an asymmetric band in the IR absorption spectrum consisting of multiple overlapping populations, the 2D IR spectrum contains multiple peak pairs, one peak pair arising from each population. In the presence of dynamic equilibrium between two populations, cross peaks will appear on the time scales of the equilibrium dynamics of the process. Although the cross peaks appear for both the blue and the red peaks, we have majorly shown the frequency range covering the blue peaks in the 2D IR spectra (Figure 3) such that cross peaks between multiple populations are clearly visible. The numerical fitting (fitting-procedure is explained later) of the 2D IR spectra was performed on the entire frequency range covering both the red and blue diagonal peaks along with the corresponding cross peaks.

**2.5. Center Line Slope Analysis.** The waiting time ($T_w$)-dependent frequency evolution known as spectral diffusion changes the correlation between the initial and final frequency. The 2D IR peaks are elongated along the diagonal, and $T_w$-dependent evolution of the 2D IR spectral line shape was modeled with the center line slope (CLS) method.[42,43] Evolution of CLS with increasing time delay is fitted with a biexponential function,

$$C(t) = a_1 e^{-(t/\tau_1)} + a_2 e^{-(t/\tau_1)}$$

**2.6. Numerical Simulation of the Linear and 2D IR Spectra.** Numerical simulations based on a full response theory treatment are performed to extract the interconversion time scales between the overlapping populations. Multiple methods have been previously reported to determine the exchange time scales which include (i) direct estimation of the cross-peak intensities/volumes from $T_w$-dependent 2D IR spectra,[44,45] (ii) modeling each peak in the $T_w$-dependent 2D IR spectra using 2D Gaussian functions,[29,46] and (iii) global fitting of the $T_w$-dependent 2D IR spectra using full response function theory.[47−49] The first two approaches have been reported for exchange involving two populations. However, the global fitting approach is generally used for two or more spectrally overlapping populations exchanging between one another. As both KSCN and $NH_4SCN$ involve exchange between three spectrally different populations, we have opted for the global fitting approach. It has been reported previously that the global fitting approach provides more accurate estimates of the exchange time scales in case of substantial overlap between the peaks.[49]

IR absorption spectra and 2D IR spectra are simulated numerically by incorporating the exchange processes during the two coherence periods ($\tau$ and $t$)[50] and the waiting time ($T_w$).[44] The details of the numerical simulations have been reported previously.[48] The static and dynamic parameters (peak positions, lifetime, anharmonicity, line widths, etc.) are obtained from experimental IR absorption and 2D IR spectra (on the model compound, e.g., MeSCN). The exchange time scales are varied to iteratively fit the IR absorption spectrum and the experimental 2D IR spectra at different $T_w$ values. Thus, a single set of parameters are fitted to IR absorption spectrum and 2D IR spectra at different time delays. Finally, the difference of the experimental and simulated spectra are calculated as shown in the Supporting Information. The goodness of the fits are calculated for both the IR absorption spectra and the 2D IR spectra. Further details on the response functions are provided in the Supporting Information. The numerical simulations are performed using Matlab.


https://doi.org/10.1021/acs.jpcb.1c08613
J. Phys. Chem. B 2022, 126, 239−248

**2.7. Quantum Chemical Calculations.** Geometries of NaSCN, KSCN, and $NH_4SCN$ contact ion pairs (CIP), dimers, and ion clusters have been optimized using density functional theory (DFT) with the hybrid functional B3LYP and the lanl2dz basis set. Frequencies of all optimized structures have been calculated by using the same functional and basis set. The effect of solvent was incorporated during geometry optimization and frequency calculations through the SMD solvation model.[51] All theoretical calculations were performed using the Gaussian 09 program.[52]

**2.8. Molecular Dynamics Simulation.** All-atom classical MD simulations were performed using the GROMACS version 2020.4 package.[53] The force field for thiocyanate anion and ammonium cation and THF were modeled using widely used AmberTools16 and ACPYPE packages using the GAFF force field.[54] Sodium and potassium cation parameters were taken from AMBER force field.[55] Multiple independent MD simulations with approximate ion concentration ranging from 5 to 100 mM were performed to check the concentration-dependent ion complex formation. LINCS algorithms were used to restrain all the covalently bonded hydrogen atoms. Periodic boundary conditions with 16 Å cut off for short-range electrostatic were implemented. The systems were first equilibrated with steepest decent energy minimization and subsequently equilibrated with velocity rescale thermostat and Parrinello−Rahman barostat. Final production runs of 10 ns were performed.

## 3. RESULTS AND DISCUSSION

**3.1. IR Absorption Spectroscopy.** The IR absorption spectrum of NaSCN in THF shows a broad asymmetric band in the nitrile stretch region (Figure 1a). The band consists of two overlapping peaks at 2056.1 and at 2042.6 $cm^{-1}$. The peak positions agree with the published reports.[36,56] The high-frequency peak has been previously assigned to contact ion pairs (CIPs) while the red-shifted peak has been attributed to contact ion-pair dimers.[36,56,57] The nitrile stretch of the $SCN^-$ anion has been reported to be sensitive to solvent, counterion, and concentration.[29,30,58−61] We have obtained IR absorption spectra of NaSCN at different concentrations (Figure S1). The low-frequency peak shows a monotonic increase with increasing solute concentrations. A concomitant decrease is observed in the high-frequency peak. As the formation of contact ion-pair dimers should increase with increasing solute concentration, the increase in the red-shifted population with increasing solute concentration corroborates the previously reported peak assignments.

Furthermore, the vibrational frequencies, calculated from DFT optimized structures, agree well with those obtained from the IR absorption experiments, confirming the relative trend in the frequencies in the dimer and the CIP (Figure 1d,g). Although thiocyanate is an ambidentate anion, the DFT calculations (Figure 1g,j), in agreement with Pearson's hard soft acid base (HSAB) theory, indicate that the nitrogen atom of the $SCN^-$ anion interacts with $Na^+$ to form the CIP. The low dielectric constant of THF is crucial for the formation of the associated complexes. It has been reported that LiSCN exists in an equilibrium between free $SCN^-$ anion and the CIP in a solvent of higher polarity than that of THF.[34] The smaller ionic radius of $Li^+$ compared to that of $Na^+$ would indicate otherwise if specific and nonspecific solute−solvent interactions had no role to play. The role of the solvent can also be observed from the vibrational frequency calculations (Table S1). Although treating the solvent as a continuum dielectric provides the correct trend in frequencies, the inclusion of explicit THF molecules is needed for a good agreement with the experimental frequencies.

It has been reported that the solubility of the alkali metal salts decreases smoothly with the increase in the ionic radius of the cation.[62] We have also observed that the solubility of the thiocyanate salts drastically decreases in THF as the counter-cation is changed from $Na^+$ to $K^+$. As $K^+$ has a larger ionic radius compared to $Na^+$ (Table S2),[63] we have further investigated KSCN in THF, albeit at a lower concentration. The IR absorption spectrum in the nitrile stretch region of KSCN shows an asymmetric band centered at ∼2055 $cm^{-1}$ in THF (Figure 1b). The spectrum could be fitted to two peaks at 2043.6 and 2050.3 $cm^{-1}$, along with a blue-shifted transition at 2059.9 $cm^{-1}$, respectively. Vibrational frequency calculations indicate that the peaks at 2043.6 and 2050.3 $cm^{-1}$ could plausibly be attributed to the ion-pair dimer (Figure 1e) and the CIP (Figure 1h). The $SCN^-$ anion forms specific interaction with the counterion in a CIP. The nitrile stretch frequency shows a monochromatic blue shift in the presence of specific interactions, where the extent of the frequency shift increases with an increase in the interaction.[64−66] Compared to $Na^+$, $K^+$ has a lower energy of interaction with the thiocyanate anion (Table S3), which can explain the red shift in the CIP peak position from NaSCN to KSCN. In a previous study, an additional transition, blue-shifted to the CIP peak, was observed and was tentatively assigned to triple ions.[56] Vibrational frequency calculations indicate that a blue-shifted transition can also arise from an S-bonded contact ion pair (Figure 1k). Given the larger polarizability of $K^+$ compared to $Na^+$, the possibility of the ambidentate anion interacting with the cation through both the nitrogen and the sulfur atoms cannot be ruled out. MD simulations with explicit solvent molecules, followed by frequency calculations, can possibly identify the origin of the blue-shifted peak. Moreover, MD simulations can also indicate any dynamic equilibrium between the different associated ion complexes.

For the $SCN^-$ anion, the lattice energies decrease with increasing ionic radii of the cations (Table S2).[62] The ionic radius and lattice energy have been proposed to modulate the solute−solvent interactions, playing a pivotal role in the formation of various associated ion complexes. However, the relation is far from simple, as has been seen for ammonium salts. Despite having a larger ionic radius and smaller lattice energy than $K^+$, $NH_4^+$ salts show much higher solubility in THF. A possible explanation of this anomalous behavior of $NH_4^+$ salts can be the formation of hydrogen bonds between the hydrogen atoms of $NH_4^+$ and the oxygen atom of THF. We have performed IR absorption experiments on $NH_4SCN$ in THF at various concentrations. Figure 1c and Figure S2 show that the nitrile stretch spectrum of $NH_4SCN$ in THF consists of three peaks, similar to what we observe for KSCN. At the lowest concentration, the spectrum is dominated by the peak at 2047.5 $cm^{-1}$, with negligible shoulders in both higher (2066.8 $cm^{-1}$) and lower frequencies (2028.2 $cm^{-1}$). With increasing salt concentration, the populations of both the red- and blue-shifted shoulders increase along with a concomitant decrease in the population of the peak at 2047.5 $cm^{-1}$ (Figure S2). However, the population of the peak at 2028.2 $cm^{-1}$ shows a small decrease at extremely high salt concentrations, whereas the peak at 2066.8 $cm^{-1}$ shows a monotonic increase. Vibrational frequency calculations indicate the peak at


https://doi.org/10.1021/acs.jpcb.1c08613
J. Phys. Chem. B 2022, 126, 239−248

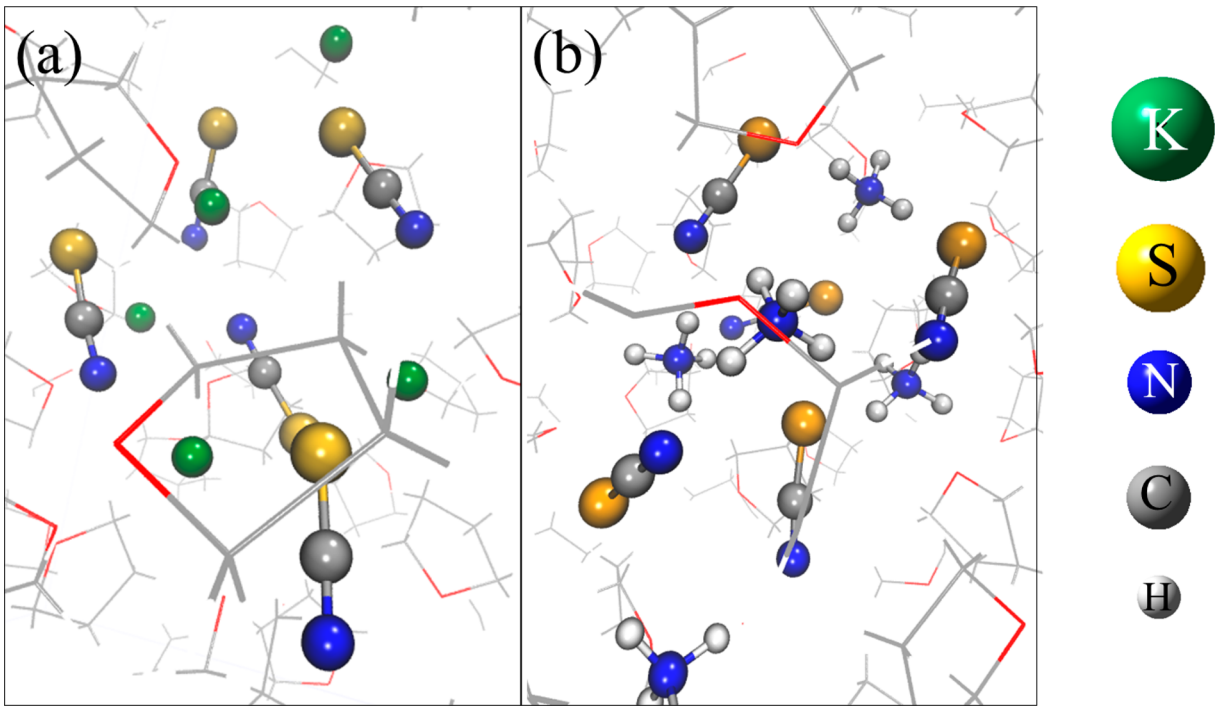


**Figure 2.** Representative snapshots of ion cluster of (a) KSCN and (b) $NH_4SCN$ from the MD simulation trajectories. The KSCN ion cluster is more loosely bound than the $NH_4SCN$ ion cluster.

2047.5 $cm^{-1}$ can arise either from free $SCN^-$ (Table S1) anion or a CIP (Figure 1i,l). As the interaction energy of $SCN^-$ anion with $NH_4^+$ is smaller than that with $K^+$, a solvent-separated ion pair is another possibility. It has been previously reported that solvent-separated ion pairs cannot be spectrally distinguished from the free $SCN^-$ anion.[34] The frequency calculations estimate the nitrile stretching frequency in the CIP to be much higher than that obtained for the predominant peak in the IR spectrum of $NH_4SCN$ at low concentrations (Figure 1i,l). However, among all cations, $NH_4^+$ should be affected the most by specific solute−solvent interactions. This is due to the possibility of the formation of hydrogen bonds between the cation and THF. In fact, calculations show a much larger decrease in the nitrile frequencies for $NH_4SCN$ compared to NaSCN or KSCN (Table S1) when few explicit solvent molecules are included along with the CIP. As only a few solvent molecules are included in the DFT optimized structures, and the nitrile frequency shows a monotonic decrease with increasing solvent molecules (Table S1), we cannot rule out the possibility of the peak at 2047.5 $cm^{-1}$ arising from the CIP. The peak at 2028.2 $cm^{-1}$ has been attributed to the ion-pair dimer as it shows an increase in population with increasing concentration of the solute. Similar to KSCN, the origin of the peak at 2066.8 $cm^{-1}$ in $NH_4SCN$ has a less definite interpretation. Interestingly, frequency calculations show that both N- and S-bonded CIPs absorb at very similar frequencies, ruling out the S-bonded CIP as the origin of the blue-shifted peak.

**3.2. Molecular Dynamics Simulations.** All-atom molecular dynamics simulation is particularly useful in getting the molecular-level picture of those phenomena by generating the data averaged over tens of nanoseconds long trajectory with explicit solvent molecules. Interestingly, previous simulation reports have shown the paramount importance of the solvent in stabilizing the ion complex and affecting the rate of association−dissociation equilibrium.[14,15] The solvent's role can further be classified by its effectiveness in screening the long-range electrostatics and its control over the degrees of freedom of the ion-complex by the manifestation of solvation dynamics. Thus, analyzing the ion complex population in the MD simulation could in turn complement the time-averaged and time-resolved information obtained from the experimental measurements.

MD simulations of the thiocyanate salt solutions with different countercations in THF further supports the diverse range of ion complex geometries. Simulation trajectories show that NaSCN forms a stable CIP and dimer in THF. Interestingly, the dynamic exchange between different subpopulations of NaSCN is found to be relatively rare in the 10 ns simulation trajectory. Contrary to NaSCN, KSCN shows the formation of loosely bound clusters along with the CIP and dimer. Both S-bonded and N-bonded CIPs are observed, which rapidly interconvert among one another. Vibrational frequency calculation shows that the nitrile frequencies in the ion cluster are blue-shifted to that of the N-bonded CIP. In comparison to $NH_4SCN$, the blue-shifted peak of KSCN in the IR absorption spectrum have a smaller frequency gap with that of the N-bonded CIP. This could indeed be possible if the ion complex structure in the solution is less compact, giving rise to a reduced blue shift due to weaker specific interaction with the cation. Representative snapshots from MD simulations (Figure 2a) visually represent the loosely held ion cluster of KSCN in THF and provide a rationale for experimental peak separations. In addition to the ion cluster, the S-bonded CIP can also contribute to the blue-shifted population.

Interestingly, simulation of ammonium thiocyanate predicts significant ion cluster formation (Figure 2b) alongside the contact ion pair and dimer. However, free thiocyanate anion was never observed during the simulation length, thereby


https://doi.org/10.1021/acs.jpcb.1c08613
J. Phys. Chem. B 2022, 126, 239−248

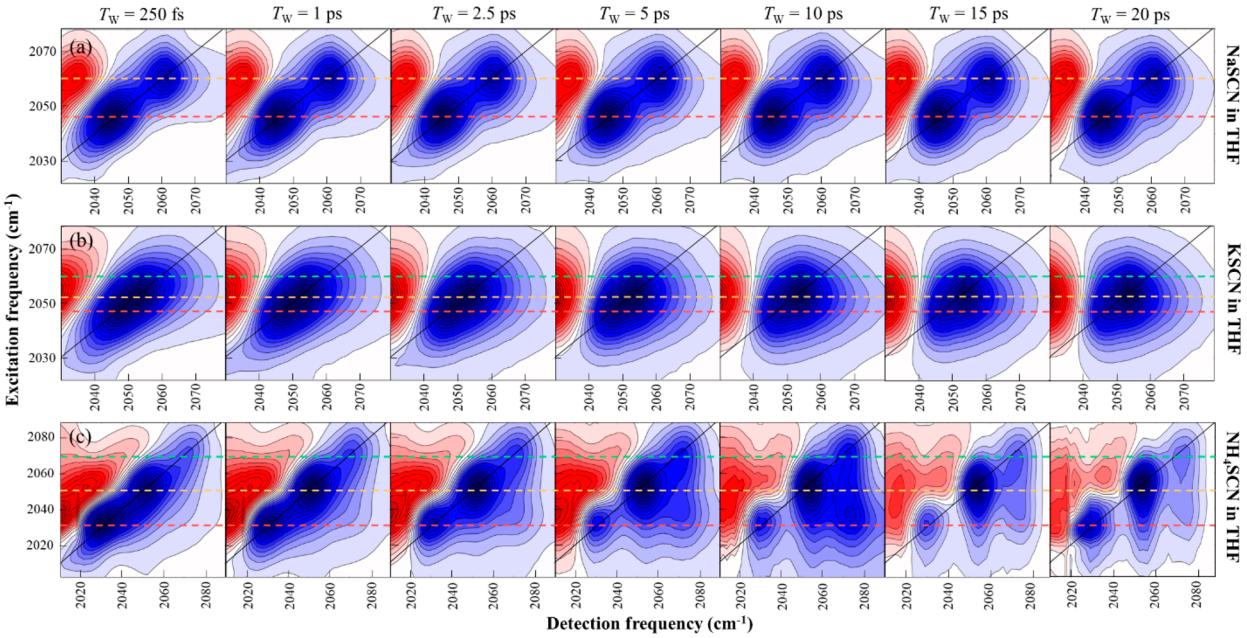


**Figure 3.** 2D IR spectra of (a) NaSCN, (b) KSCN, and (c) $NH_4SCN$ at different values of $T_w$ (250 fs, 1 ps, 2.5 ps, 5 ps, 10 ps, 15 ps, and 20 ps). The dashed lines denote the excitation frequencies of the underlying transitions arising from ion-pair dimer (red), contact ion pair (yellow), and ion cluster (green).

confirming the peak at 2047.5 cm$^{-1}$ arises from the CIP. Frequency calculation of the cluster reveals blue-shifted transitions around ∼2060−2100 cm$^{-1}$ (Table S1). Moreover, the propensity of cluster formation increases with increasing concentration of the solute. Based on this result, we can assign the blue-shifted peak in the IR absorption spectra of $NH_4SCN$ in THF to an ion cluster. In the IR absorption spectrum, the blue-shifted peak shows a monotonic increase in population with increasing solute concentration, while the red-shift peak population decreases after ∼140 mM. This trend can be explained if we consider the dimers corresponding to the red-shifted peak associate to form an ion cluster at a very high solute concentration. In fact, interconversion between different ion complexes is observed along the simulation trajectory. Both N-bound and S-bound thiocyanate population can be observed throughout the simulation. DFT analysis predicts that both the coordination modes have similar frequencies and are virtually indistinguishable in experimental spectra.

**3.3. Two-Dimensional Infrared Spectroscopy.** IR absorption spectra show that the nitrile stretch is sensitive to the formation of different associated ion complexes. Apart from deciphering the identities of these complexes, MD simulations indicate the presence of dynamic equilibria between the different ion complexes of $NH_4SCN$ and KSCN. However, such exchanging populations could not be identified between the CIP and the dimer of NaSCN. 2D IR spectroscopy can provide spectral signatures of the interchanging population in the form of $T_w$-dependent cross peaks. We have performed 2D IR spectroscopy on the different ionic electrolytes dissolved in THF. The 2D IR spectra of NaSCN show two peaks along the diagonal (Figure 3a). The peaks at the higher (dashed yellow line) and lower frequencies (dashed red line) arise from the NaSCN CIP and an ion-pair dimer. The $T_w$-dependent spectra show no cross peak (even at 130 ps, see Figure S3 of the Supporting Information), indicating the lack of any dynamic equilibrium between the NaSCN dimer and the CIP within the experimental time window. Interestingly, a previous work on LiSCN in a polar solvent (DMF) reported that free anion and the CIP interconvert at a time scale of 88 ps. The absence of cross peaks for NaSCN indicates a stronger cation−anion interaction in a low dielectric medium (THF), plausibly due to ineffective dielectric screening by the medium. At a short waiting time (250 fs), the higher-frequency peak of 70 mM NaSCN is less intense than the lower-frequency one. A similar trend is seen in the IR absorption spectrum but with a smaller intensity difference. Our calculations predict that the dimer has a higher molar extinction coefficient ($\varepsilon$) than the N-bonded CIP. It is well-known that $\varepsilon$ is related to the square of the transition dipole strength ($\vec{\mu}$). 2D IR spectroscopy is more sensitive to structural changes than IR absorption spectroscopy as 2D IR signals are proportional to $|\vec{\mu}^4|$, unlike $|\vec{\mu}^2|$ in FTIR.[67] Therefore, the increase in the relative peak intensities in the 2D IR spectrum corroborates the ab initio calculations of NaSCN and provides additional experimental support regarding the origin of the peaks. We have further performed 2D IR experiments at a different concentrations of NaSCN (30 mM, Figure S4a). Although the relative intensities of the diagonal peaks change with changes in the solute concentration, the absence of cross peaks indicates that the populations are not interchanging within the experimental time window.

The 2D IR spectra of KSCN surprisingly show a single peak along the diagonal (Figure 3b). The three FTIR peaks of KSCN (Figure 1b) are closer to one another than those observed for NaSCN and $NH_4SCN$ (Figure 1a,c). A combination of the small frequency gaps between the three peaks and different molar extinction coefficients for different populations can lead to a single peak in the 2D IR spectrum. It is to be noted that the single peak in the 2D IR spectrum of KSCN almost spreads over the combined frequency range of the two peaks in the 2D IR spectra of NaSCN, indicating the plausible presence of multiple underlying populations. The shape of the spectrum indicates the presence of a cross peak at a large waiting times. To investigate any presence of a dynamic


https://doi.org/10.1021/acs.jpcb.1c08613
J. Phys. Chem. B 2022, 126, 239−248

equilibrium between the ion complexes, we have iteratively fitted the IR absorption and the $T_w$-dependent 2D IR spectra using a full response function theory to determine the exchange time scales (Figure S5). Interestingly, our numerical simulation shows that the loosely held cluster interconverts either to a CIP or a dimer at ∼10 ps time scales. However, the interconversion between the CIP and dimer occurs at a slower time scale (∼40 ps).

Figure 3c shows the $T_w$-dependent 2D IR spectra of $NH_4SCN$ in THF. Three distinct diagonally elongated peaks can be observed along the diagonal at a shorter waiting time. In the order of descending frequencies, the peaks correspond to the ion cluster, CIP, and dimer. Apart from the three diagonal peaks, three off-diagonal cross peaks appear with increasing waiting times. In Figure 3c, the cross peak between the dimer and the CIP appears at (2028 $cm^{-1}$, 2047 $cm^{-1}$). The dimer−cluster and the CIP−cluster cross peaks appear at (2028 $cm^{-1}$, 2067 $cm^{-1}$) and (2047 $cm^{-1}$, 2067 $cm^{-1}$). The time evolution of the cross-peaks indicates interchange between all different populations in $NH_4SCN$. Unlike in KSCN, the large frequency spacing between the diagonal peaks makes the cross peaks distinguishable at large waiting times. The overlap of the dimer diagonal peak at (2028 $cm^{-1}$, 2028 $cm^{-1}$) with the CIP−dimer cross peak arising from v = 1 to v = 2 transition apparently reduces the diagonal peak intensity at larger waiting times.

The complicated dynamic equilibria do not allow us to estimate the different exchange rates based on fitting the peak volumes to a mathematical model.[44,68] To quantitatively analyze the interconversion dynamics between a pair of ion complexes, we have performed iterative least-squares fitting of the corresponding numerically simulated 2DIR spectrum (Figures S6).[48,69] The conversion of the CIP to a dimer is estimated to occur at a 23 ps time scale, whereas the cluster can convert to a dimer or a CIP at much faster time scales. The cluster to the CIP and cluster to the dimer time scales are 11 and 7 ps, respectively.

$NH_4SCN$ has been recently reported to be used as a dopant salt in polymer electrolytes based electrochemical devices, and the ion complexation dynamics have been linked with the overall conductivity.[70] Interestingly, $NH_4SCN$ has a strong effect on polymer electrolytes dielectric constant and has been hypothesized to be dependent on association and dissociation dynamics.[71] Thus, quantifying the complexation dynamics provides a molecular picture for more complex electrolyte systems.

To understand the role of the solvent in the dynamic equilibria, we have performed additional 2D IR experiments on methyl thiocyanate (MeSCN) in THF. MeSCN, being a neutral molecule, cannot form the different ion complexes in THF and show a single peak both in the IR absorption and 2D IR spectra (Figure S7). Analysis of the $T_w$-dependent change in the peak shape using CLS formalism provides the fluctuation time scales of THF. The CLS could be fitted to a biexponential decay, which provides the time scales of ∼0.5 ps and ∼10 ps (Figure S7). This result is in agreement with the CLS decay time scale obtained for NaSCN in THF. Intriguingly, the slower time scale matches with that of dynamic equilibrium involving the cluster and the CIP/dimer either in KSCN or $NH_4SCN$.

The slower solvent fluctuation time scale is attributed to the exchange of the solvent molecules between the first and second solvation shells.[42,58] As THF coordinates with the $NH_4^+$ cation, we surmise that exchange within two solvation shells can destabilize few $NH_4SCN$ molecules of the cluster, resulting in dissociation of a CIP or dimer from the cluster. Therefore, the cluster−dimer and cluster−CIP exchange time scales show good agreement with the solvent exchange time scale of THF. On the other hand, the effect of solvent exchange will be less severe for a dimer−CIP equilibrium as these smaller-sized complexes are better solvated by multiple THF molecules, leading to a slower exchange time scale.

## 4. CONCLUSION

In this work, we have shown that the vibrational signature of thiocyanate ion is an excellent reporter of different ion-specific cation−anion complexes in a low dielectric medium. Depending on the nature of the cation ($Na^+$, $K^+$ and $NH_4^+$), the changes in the relative population of the ion complexes are manifested in the peaks of the IR absorption spectra. For example, the contact ion pair and the dimer of NaSCN in THF absorb at 2056.1 and 2042.6 $cm^{-1}$, respectively. This peak assignment agrees well with the literature and could be further supported by vibrational frequency calculations on the DFT optimized structures.

The lower interaction energy of $K^+$ with the anion induces a weak specific interaction in the CIP, resulting in a smaller red shift compared to that in NaSCN. 2D IR spectra of KSCN indicate the presence of multiple closely separated ion complex populations hidden inside a broad diagonal peak. Possible chemical exchange between various ion complexes at a longer waiting time is indicated by the 2D IR spectral shape. Quantitative analysis of such population exchange rates shows that interconversion rates involving ion clusters are mediated by solvent fluctuations. Interestingly, the signature of such cross peaks could not be seen in the 2D IR spectra of NaSCN within the experimental waiting time window.

For $NH_4SCN$, the nitrile stretch is split into three peaks around 2047.5 $cm^{-1}$. Two of the peaks are attributed to the CIP and dimer based on the vibrational frequency analysis. However, MD simulations predict significant cluster formation. Frequency calculation of such cluster population matches well with the blue-shifted peak in the linear IR spectra. The estimated ultrafast interconversion rates between the ion cluster and ion pair (11 ps) and between the ion cluster and dimer (7 ps) from 2D IR show similar time scale. However, the interconversion between ion pair and dimer (23 ps) is much slower. This result was further rationalized in terms of solvent fluctuation mediated by the dynamic equilibrium of the ion complexes as the long component of the solvation dynamics time scale matches with the association−dissociation rate of the former two complexes.

Our results demonstrate that a combination of multiple experimental and theoretical techniques can provide a molecular-level understanding of the unique ion clusters formed by the different ionic electrolytes in a low dielectric medium solvent. We also show that the association−dissociation rates of the dynamic equilibrium among the various molecular species can be estimated from 2D IR spectroscopy. The estimation of these rates is significant as they are related to the lifetimes of the ion complexes, thereby providing us a fundamental understanding about the ion transport as a function of the cations.


https://doi.org/10.1021/acs.jpcb.1c08613
J. Phys. Chem. B 2022, 126, 239−248

## ■ ASSOCIATED CONTENT

### Supporting Information

The Supporting Information is available free of charge at https://pubs.acs.org/doi/10.1021/acs.jpcb.1c08613.

Concentration-dependent IR absorption spectra of different SCN salts, experimental and simulated 2D IR spectra, FTIR and 2D IR spectra of MeSCN in THF, optimized geometries and calculated stretching frequencies, energies and ionic radii, parameters used for numerical simulation, Feynman diagrams, results of DFT calculations, 2D IR simulation details (PDF)

## ■ AUTHOR INFORMATION


### Corresponding Authors

**Yung Sam Kim** − *Department of Chemistry, Ulsan National Institute of Science and Technology (UNIST), Ulsan 44919, Korea;* orcid.org/0000-0001-6306-7438; Email: kimys@unist.ac.kr

**Sayan Bagchi** − *Physical and Materials Chemistry Division, CSIR-National Chemical Laboratory, Pune 411008, India; Academy of Scientific and Innovative Research (AcSIR), Ghaziabad 201002, India;* orcid.org/0000-0001-6932-3113; Email: s.bagchi@ncl.res.in

### Authors

**Deborin Ghosh** − *Physical and Materials Chemistry Division, CSIR-National Chemical Laboratory, Pune 411008, India*

**Sushil S. Sakpal** − *Physical and Materials Chemistry Division, CSIR-National Chemical Laboratory, Pune 411008, India; Academy of Scientific and Innovative Research (AcSIR), Ghaziabad 201002, India*

**Srijan Chatterjee** − *Physical and Materials Chemistry Division, CSIR-National Chemical Laboratory, Pune 411008, India; Academy of Scientific and Innovative Research (AcSIR), Ghaziabad 201002, India;* orcid.org/0000-0001-9701-4158

**Samadhan H. Deshmukh** − *Physical and Materials Chemistry Division, CSIR-National Chemical Laboratory, Pune 411008, India; Academy of Scientific and Innovative Research (AcSIR), Ghaziabad 201002, India*

**Hyejin Kwon** − *Department of Chemistry, Ulsan National Institute of Science and Technology (UNIST), Ulsan 44919, Korea*

Complete contact information is available at: https://pubs.acs.org/10.1021/acs.jpcb.1c08613


### Notes

The authors declare no competing financial interest.

## ■ ACKNOWLEDGMENTS

S.B. thanks CSIR-NCL and SERB, India (SR/S2/RJN-142/2012 and EMR/2016/000576), for financial support. D.G. acknowledges SERB India (PDF/2018/000046) for financial support. The support and the resources provided by the "PARAM Brahma Facility" under the National Supercomputing Mission, Government of India, at the Indian Institute of Science Education and Research (IISER) Pune are gratefully acknowledged. S.S.S. acknowledges UGC and S.H.D acknowledges CSIR for research fellowships. This work was also supported by National Research Foundation of Korea (2018R1D1A1A02086153) to Y.S.K.

## ■ REFERENCES


(1) Xie, L.; Ilic, M. D. Model Predictive Dispatch in Electric Energy Systems with Intermittent Resources, *IEEE International Conference on Systems, Man and Cybernetics*, **2008**, 42−47.

(2) Ellis, B. L.; Nazar, L. F. Sodium and Sodium-Ion Energy Storage Batteries. *Curr. Opin. Solid State Mater. Sci.* **2012**, *16*, 168−177.

(3) Tarascon, J. M.; Armand, M. Issues and Challenges Facing Rechargeable Lithium Batteries. *Nature* **2001**, *414*, 359−367.

(4) Xu, K. Nonaqueous Liquid Electrolytes for Lithium-Based Rechargeable Batteries. *Chem. Rev.* **2004**, *104*, 4303−4418.

(5) Goodenough, J. B.; Park, K.-S. The Li-Ion Rechargeable Battery: A Perspective. *J. Am. Chem. Soc.* **2013**, *135*, 1167−1176.

(6) Wang, L.; Zhao, Y.; Fan, B.; Carta, M.; Malpass-Evans, R.; McKeown, N. B.; Marken, F. Polymer of Intrinsic Microporosity (PIM) Films and Membranes in Electrochemical Energy Storage and Conversion: A Mini-Review. *Electrochem. Commun.* **2020**, *118*, 106798.

(7) Kushner, D. I.; Crothers, A. R.; Kusoglu, A.; Weber, A. Z. Transport Phenomena in Flow Battery Ion-conducting Membranes. *Curr. Opin. Electrochem.* **2020**, *21*, 132−139.

(8) Choo, Y.; Halat, D. M.; Villaluenga, I.; Timachova, K.; Balsara, N. P. Diffusion and Migration in Polymer Electrolytes. *Prog. Polym. Sci.* **2020**, *103*, 101220.

(9) Evans, J.; Vincent, C. A.; Bruce, P. G. Electrochemical Measurement of Transference Numbers in Polymer Electrolytes. *Polymer* **1987**, *28*, 2324−2328.

(10) Rehm, T. H.; Schmuck, C. Ion-Pair Induced Self-Assembly in Aqueous Solvents. *Chem. Soc. Rev.* **2010**, *39*, 3597−3611.

(11) Brak, K.; Jacobsen, E. N. Asymmetric Ion-Pairing Catalysis. *Angew. Chem., Int. Ed.* **2013**, *52*, 534−561.

(12) Huang, Y.; Liang, Z.; Wang, H. A Dual-Ion Battery Has Two Sides: The Effect of Ion-Pairs. *Chem. Commun.* **2020**, *56*, 10070−10073.

(13) Marcus, Y.; Hefter, G. Ion Pairing. *Chem. Rev.* **2006**, *106*, 4585−4621.

(14) Self, J.; Hahn, N. T.; Fong, K. D.; McClary, S. A.; Zavadil, K. R.; Persson, K. A. Ion Pairing and Redissociaton in Low-Permittivity Electrolytes for Multivalent Battery Applications. *J. Phys. Chem. Lett.* **2020**, *11*, 2046−2052.

(15) Gudla, H.; Shao, Y.; Phunnarungsi, S.; Brandell, D.; Zhang, C. Importance of the Ion-Pair Lifetime in Polymer Electrolytes. *J. Phys. Chem. Lett.* **2021**, *12*, 8460−8464.

(16) Shen, K.-H.; Hall, L. M. Effects of Ion Size and Dielectric Constant on Ion Transport and Transference Number in Polymer Electrolytes. *Macromolecules* **2020**, *53*, 10086−10096.

(17) Bocharova, V.; Sokolov, A. P. Perspectives for Polymer Electrolytes: A View from Fundamentals of Ionic Conductivity. *Macromolecules* **2020**, *53*, 4141−4157.

(18) Shen, K.-H.; Hall, L. M. Ion Conductivity and Correlations in Model Salt-Doped Polymers: Effects of Interaction Strength and Concentration. *Macromolecules* **2020**, *53*, 3655−3668.

(19) Kisliuk, A.; Bocharova, V.; Popov, I.; Gainaru, C.; Sokolov, A. P. Fundamental Parameters Governing Ion Conductivity in Polymer Electrolytes. *Electrochim. Acta* **2019**, *299*, 191−196.

(20) Popov, I.; Biernacka, K.; Zhu, H.; Nti, F.; Porcarelli, L.; Wang, X.; Khamzin, A.; Gainaru, C.; Forsyth, M.; Sokolov, A. P. Strongly Correlated Ion Dynamics in Plastic Ionic Crystals and Polymerized Ionic Liquids. *J. Phys. Chem. C* **2020**, *124*, 17889−17896.

(21) Tomšič, M.; Bešter-Rogač, M.; Jamnik, A.; Neueder, R.; Barthel, J. Conductivity of Magnesium Sulfate in Water from 5 to 35°C and from Infinite Dilution to Saturation. *J. Solution Chem.* **2002**, *31*, 19−31.

(22) Barthel, J.; Buchner, R.; Eberspächer, P. N.; Münsterer, M.; Stauber, J.; Wurm, B. Dielectric Relaxation Spectroscopy of Electrolyte Solutions. Recent Developments and Prospects. *J. Mol. Liq.* **1998**, *78*, 83−109.

(23) Wachter, W.; Fernandez, Š.; Buchner, R.; Hefter, G. Ion Association and Hydration in Aqueous Solutions of LiCl and $Li_2SO_4$ by Dielectric Spectroscopy. *J. Phys. Chem. B* **2007**, *111*, 9010−9017.

(24) Le Borgne, C.; Illien, B.; Beignon, M.; Chabanel, M. Ion Association of Alkali and Alkaline Earth Metal Azides in Dimethylsulfoxide. Infrared Spectrometry and Ab-Initio Calculations. *Phys. Chem. Chem. Phys.* **1999**, *1*, 4701−4706.
(25) Barthel, J.; Buchner, R.; Wismeth, E. FTIR Spectroscopy of Ion Solvation of $LiClO_4$ and LiSCN in Acetonitrile, Benzonitrile, and Propylene Carbonate. *J. Solution Chem.* **2000**, *29*, 937−954.
(26) Kwon, Y.; Park, S. Complexation Dynamics of $CH_3SCN$ and $Li^+$ in Acetonitrile Studied by Two-Dimensional Infrared Spectroscopy. *Phys. Chem. Chem. Phys.* **2015**, *17*, 24193−24200.
(27) Moilanen, D. E.; Wong, D.; Rosenfeld, D. E.; Fenn, E. E.; Fayer, M. D. Ion−Water Hydrogen-Bond Switching Observed With 2D IR Vibrational Echo Chemical Exchange Spectroscopy. *Proc. Natl. Acad. Sci. U. S. A.* **2009**, *106*, 375−380.
(28) Ji, M.; Odelius, M.; Gaffney, K. J. Large Angular Jump Mechanism Observed for Hydrogen Bond Exchange in Aqueous Perchlorate Solution. *Science* **2010**, *328*, 1003−1005.
(29) Yuan, R.; Yan, C.; Fayer, M. Ion−Molecule Complex Dissociation and Formation Dynamics in LiCl Aqueous Solutions from 2D IR Spectroscopy. *J. Phys. Chem. B* **2018**, *122*, 10582−10592.
(30) Park, K. H.; Choi, S. R.; Choi, J. H.; Park, S.; Cho, M. Real-Time Probing of Ion Pairing Dynamics With 2DIR Spectroscopy. *ChemPhysChem* **2010**, *11*, 3632−3637.
(31) Sun, Z.; Zhang, W.; Ji, M.; Hartsock, R.; Gaffney, K. J. Aqueous $Mg^{2+}$ and $Ca^{2+}$ Ligand Exchange Mechanisms Identified with 2DIR Spectroscopy. *J. Phys. Chem. B* **2013**, *117*, 12268−12275.
(32) Gaffney, K. J.; Ji, M.; Odelius, M.; Park, S.; Sun, Z. H-Bond Switching and Ligand Exchange Dynamics in Aqueous Ionic Solution. *Chem. Phys. Lett.* **2011**, *504*, 1−6.
(33) Sun, Z.; Zhang, W.; Ji, M.; Hartsock, R.; Gaffney, K. J. Contact Ion Pair Formation between Hard Acids and Soft Bases in Aqueous Solutions Observed with 2DIR Spectroscopy. *J. Phys. Chem. B* **2013**, *117*, 15306−15312.
(34) Lee, K.-K.; Park, K.-H.; Kwon, D.; Choi, J.-H.; Son, H.; Park, S.; Cho, M. Ion-Pairing Dynamics of $Li^+$ and $SCN^-$ in Dimethylformamide Solution: Chemical Exchange Two-Dimensional Infrared Spectroscopy. *J. Chem. Phys.* **2011**, *134*, 064506.
(35) Ji, M.; Park, S.; Gaffney, K. J. Dynamics of Ion Assembly in Solution: 2DIR Spectroscopy Study of LiNCS in Benzonitrile. *J. Phys. Chem. Lett.* **2010**, *1*, 1771−1775.
(36) Kiefer, L. M.; Kubarych, K. J. NOESY-Like 2D-IR Spectroscopy Reveals Non-Gaussian Dynamics. *J. Phys. Chem. Lett.* **2016**, *7*, 3819−3824.
(37) Geissler, P. L.; Dellago, C.; Chandler, D. Kinetic Pathways of Ion Pair Dissociation in Water. *J. Phys. Chem. B* **1999**, *103*, 3706−3710.
(38) Fennell, C. J.; Bizjak, A.; Vlachy, V.; Dill, K. A. Ion Pairing in Molecular Simulations of Aqueous Alkali Halide Solutions. *J. Phys. Chem. B* **2009**, *113*, 6782−6791.
(39) Baskin, A.; Prendergast, D. Ion Solvation Engineering: How to Manipulate the Multiplicity of the Coordination Environment of Multivalent Ions. *J. Phys. Chem. Lett.* **2020**, *11*, 9336−9343.
(40) Lim, L. H. V.; Pribil, A. B.; Ellmerer, A. E.; Randolf, B. R.; Rode, B. M. Temperature Dependence of Structure and Dynamics of the Hydrated $Ca^{2+}$ Ion According to Ab Initio Quantum Mechanical Charge Field and Classical Molecular Dynamics. *J. Comput. Chem.* **2009**, *31*, 1195−1200.
(41) Bian, H.; Chen, H.; Zhang, Q.; Li, J.; Wen, X.; Zhuang, W.; Zheng, J. Cation Effects on Rotational Dynamics of Anions and Water Molecules in Alkali ($Li^+$, $Na^+$, $K^+$, $Cs^+$) Thiocyanate ($SCN^-$) Aqueous Solutions. *J. Phys. Chem. B* **2013**, *117*, 7972−7984.
(42) Chatterjee, S.; Ghosh, D.; Haldar, T.; Deb, P.; Sakpal, S. S.; Deshmukh, S. H.; Kashid, S. M.; Bagchi, S. Hydrocarbon Chain-Length Dependence of Solvation Dynamics in Alcohol-Based Deep Eutectic Solvents: A Two-Dimensional Infrared Spectroscopic Investigation. *J. Phys. Chem. B* **2019**, *123*, 9355−9363.
(43) Kwak, K.; Park, S.; Finkelstein, I. J.; Fayer, M. D. Frequency-Frequency Correlation Functions and Apodization in Two-Dimensional Infrared Vibrational Echo Spectroscopy: A New Approach. *J. Chem. Phys.* **2007**, *127*, 124503.
(44) Kim, Y. S.; Hochstrasser, R. M. Chemical Exchange 2D IR of Hydrogen-Bond Making and Breaking. *Proc. Natl. Acad. Sci. U. S. A.* **2005**, *102*, 11185−11190.
(45) Bagchi, S.; Charnley, A. K.; Smith, A. B.; Hochstrasser, R. M. Equilibrium Exchange Processes of the Aqueous Tryptophan Dipeptide. *J. Phys. Chem. B* **2009**, *113*, 8412−8417.
(46) Yuan, R.; Fayer, M. D. Dynamics of Water Molecules and Ions in Concentrated Lithium Chloride Solutions Probed with Ultrafast 2D IR Spectroscopy. *J. Phys. Chem. B* **2019**, *123*, 7628−7639.
(47) Deb, P.; Jin, G. Y.; Singh, S. K.; Moon, J.; Kwon, H.; Das, A.; Bagchi, S.; Kim, Y. S. Interconverting Hydrogen-Bonding and Weak n $\rightarrow$ $\pi^*$ Interactions in Aqueous Solution: A Direct Spectroscopic Evidence. *J. Phys. Chem. Lett.* **2018**, *9*, 5425−5429.
(48) Kashid, S. M.; Jin, G. Y.; Bagchi, S.; Kim, Y. S. Cosolvent Effects on Solute−Solvent Hydrogen-Bond Dynamics: Ultrafast 2D IR Investigations. *J. Phys. Chem. B* **2015**, *119*, 15334−15343.
(49) Kübel, J.; Lee, G.; Ooi, S. A.; Westenhoff, S.; Han, H.; Cho, M.; Maj, M. Ultrafast Chemical Exchange Dynamics of Hydrogen Bonds Observed via Isonitrile Infrared Sensors: Implications for Biomolecular Studies. *J. Phys. Chem. Lett.* **2019**, *10*, 7878−7883.
(50) Kim, Y. S.; Hochstrasser, R. M. Comparison of Linear and 2D IR Spectra in the Presence of Fast Exchange. *J. Phys. Chem. B* **2006**, *110*, 8531−8534.
(51) Marenich, A. V.; Cramer, C. J.; Truhlar, D. G. Universal Solvation Model Based on Solute Electron Density and on a Continuum Model of the Solvent Defined by the Bulk Dielectric Constant and Atomic Surface Tensions. *J. Phys. Chem. B* **2009**, *113*, 6378−6396.
(52) Frisch, M. J. T., G. W; Schlegel, H. B.; Scuseria, G. E.;; Robb, M. A. C., J. R; Scalmani, G.; Barone, V.; Mennucci, B.; Petersson, G. A.; et al. *Gaussion 09*, A.01; Gaussian, Inc.: Wallingford, CT, 2009.
(53) Abraham, M. J.; Murtola, T.; Schulz, R.; Páll, S.; Smith, J. C.; Hess, B.; Lindahl, E. GROMACS: High Performance Molecular Simulations Through Multi-Level Parallelism From Laptops to Supercomputers. *Softwarex* **2015**, *1*, 19−25.
(54) Sousa da Silva, A. W.; Vranken, W. F. ACPYPE - AnteChamber Python Parser interface. *BMC Res. Notes* **2012**, *5*, 367.
(55) Wang, J.; Wolf, R. M.; Caldwell, J. W.; Kollman, P. A.; Case, D. A. Development and Testing of a General Amber Force Field. *J. Comput. Chem.* **2004**, *25*, 1157−1174.
(56) Saar, D.; Petrucci, S. Infrared and Ultrasonic Spectra of Sodium Thiocyanate and Lithium Thiocyanate in Tetrahydrofuran. *J. Phys. Chem.* **1986**, *90*, 3326−3330.
(57) Paoli, D.; Luçon, M.; Chabanel, M. Vibrational Study of Ionic Association in Aprotic Solvents—I. The Ion Pairs of Alkali and Silver Thiocyanate in Dimethylformamide or Dimethylthioformamide. *Spectrochim. Acta A Mol. Biomol. Spectrosc.* **1978**, *34*, 1087−1091.
(58) Cui, Y.; Fulfer, K. D.; Ma, J.; Weldeghiorghis, T. K.; Kuroda, D. G. Solvation Dynamics of an Ionic Probe in Choline Chloride-Based Deep Eutectic Solvents. *Phys. Chem. Chem. Phys.* **2016**, *18*, 31471−31479.
(59) Sakpal, S. S.; Deshmukh, S. H.; Chatterjee, S.; Ghosh, D.; Bagchi, S. Transition of a Deep Eutectic Solution to Aqueous Solution: A Dynamical Perspective of the Dissolved Solute. *J. Phys. Chem. Lett.* **2021**, *12*, 8784−8789.
(60) Ren, Z.; Brinzer, T.; Dutta, S.; Garrett-Roe, S. Thiocyanate as a Local Probe of Ultrafast Structure and Dynamics in Imidazolium-Based Ionic Liquids: Water-Induced Heterogeneity and Cation-Induced Ion Pairing. *J. Phys. Chem. B* **2015**, *119*, 4699−4712.
(61) Johnson, C. A.; Parker, A. W.; Donaldson, P. M.; Garrett-Roe, S. An Ultrafast Vibrational Study of Dynamical Heterogeneity in the Protic Ionic Liquid Ethyl-Ammonium Nitrate. I. Room Temperature Dynamics. *J. Chem. Phys.* **2021**, *154*, 134502.
(62) Hála, J.; Tuck, D. G. Solubility of Alkali Metal and Ammonium Thiocyanates and Iodides in Tri-N-Butyl Phosphate. *Can. J. Chem.* **1970**, *48*, 2843−2846.


https://doi.org/10.1021/acs.jpcb.1c08613
J. Phys. Chem. B 2022, 126, 239−248

(63) Wells, A. F. *Structural inorganic chemistry*; Oxford University Press: 1962.
(64) Deb, P.; Haldar, T.; Kashid, S. M.; Banerjee, S.; Chakrabarty, S.; Bagchi, S. Correlating Nitrile IR Frequencies to Local Electrostatics Quantifies Noncovalent Interactions of Peptides and Proteins. *J. Phys. Chem. B* **2016**, *120*, 4034−4046.
(65) Bagchi, S.; Fried, S. D.; Boxer, S. G. A Solvatochromic Model Calibrates Nitriles' Vibrational Frequencies to Electrostatic Fields. *J. Am. Chem. Soc.* **2012**, *134*, 10373−10376.
(66) Fafarman, A. T.; Sigala, P. A.; Herschlag, D.; Boxer, S. G. Decomposition of Vibrational Shifts of Nitriles into Electrostatic and Hydrogen-Bonding Effects. *J. Am. Chem. Soc.* **2010**, *132*, 12811−12813.
(67) Dunkelberger, E. B.; Grechko, M.; Zanni, M. T. Transition Dipoles from 1D and 2D Infrared Spectroscopy Help Reveal the Secondary Structures of Proteins: Application to Amyloids. *J. Phys. Chem. B* **2015**, *119*, 14065−14075.
(68) Zheng, J.; Kwak, K.; Asbury, J.; Chen, X.; Piletic, I. R.; Fayer, M. D. Ultrafast Dynamics of Solute-Solvent Complexation Observed at Thermal Equilibrium in Real Time. *Science* **2005**, *309*, 1338−1343.
(69) Kashid, S. M.; Jin, G. Y.; Chakrabarty, S.; Kim, Y. S.; Bagchi, S. Two-Dimensional Infrared Spectroscopy Reveals Cosolvent-Composition-Dependent Crossover in Intermolecular Hydrogen-Bond Dynamics. *J. Phys. Chem. Lett.* **2017**, *8*, 1604−1609.
(70) Shamsuri, N. A.; Zaine, S. N. A.; Yusof, Y. M.; Yahya, W. Z. N.; Shukur, M. F. Effect of Ammonium Thiocyanate on Ionic Conductivity and Thermal Properties of Polyvinyl Alcohol−Methylcellulose−Based Polymer Electrolytes. *Ionics* **2020**, *26*, 6083−6093.
(71) Zulkefli, F. N.; Navaratnam, S.; Ahmad, A. H. Proton Conducting Biopolymer Electrolytes Based on Starch Incorporated with Ammonium Thiocyanate. *Adv. Mater. Res.* **2015**, *1112*, 275−278.




https://doi.org/10.1021/acs.jpcb.1c08613
*J. Phys. Chem. B* 2022, 126, 239−248